A new approach to vision-based robot control with omni-directional cameras

S. Benhimane, Ezio Malis

A new approach to vision-based robot control with omni-directional cameras

Selim BENHIMANE

INRIA Sophia Antipolis, FRANCE
Selim.Benhimane@sophia.inria.fr

Ezio MALIS

INRIA Sophia Antipolis, FRANCE
Ezio.Malis@sophia.inria.fr

Abstract— In the last decade, research on vision-based robot control has been concentrated on two main issues: the narrow field of view of the conventional camera and the model dependency of the standard visual servoing approaches. In this paper, we propose a simple and elegant solution to these issues. To enlarge the field of view of the cameras, we use omni-directional cameras. And to overcome the model dependency problem, we propose a new visual servoing method for omni-directional cameras that does not need any measure of the 3D structure of the observed target with respect to which the visual servoing is performed. Only visual information measured from the reference and the current images are needed in order to compute a task function isomorphic to the camera pose and to compute the control law to be applied to the robot. We provide the theoretical proof of the existence of the isomorphism and the theoretical proof of the local stability of the control law.

I. INTRODUCTION

Visual servoing is a robotic task that consists in controlling a robot thanks to visual information acquired by one or multiple cameras [14], [15]. This robotic task can be considered as the regulation of a task function $\mathbf{e}(\mathbf{q}, t)$ that depends on the robot configuration $\mathbf{q}$ and the time t [23]. In the last decade, research in this field has been concentrated on two main issues.

The first issue is the design of control laws that keep as much as possible the target in the field of view of the camera. This problem, has been extensively investigated since standard perspective cameras have limited fields of view. Several solutions have been proposed: "ad hoc" visual servoing schemes [7], path planning [20], use of zooming camera [5]. In addition, the use of omni-directional systems has considerably enlarged the field of view of standard cameras.

The second issue concerns the design of control laws that rely as less as possible on accurate calibration (e.g. the camera intrinsic parameters) and as less as possible on measure of the structure of the target (e.g. a 3D model). In the literature, visual servoing schemes are generally classified as follows:

- 3D visual servoing: the task function $\mathbf{e}(\mathbf{q}, t)$ is expressed in the Cartesian space, i.e. the visual information acquired from the two images (the reference and the current images) are used to reconstruct explicitly the pose (the translation and the rotation in the Cartesian space) of the camera (see for example [4], [25], [17]). The advantage of an explicit estimation of the error in the Cartesian space is the decoupling of the task function, i.e. the camera rotation and the camera translation can be controlled independently from each other. The camera translation (up to a scale factor) and the camera rotation can be estimated through the Essential matrix [16], [10], [24], [12]. However, the Essential matrix degenerates (it can not be estimated) when the target is planar or when the motion done by the camera between the reference and the current pose is a pure rotation. For these reasons, it is better to estimate the camera translation (up to a scale factor) and the camera rotation using a homography matrix [18], [13].

- 2D visual servoing: the task function $\mathbf{e}(\mathbf{q}, t)$ is expressed directly in the image, i.e. these visual servoing methods do not need the explicit estimation of the pose error in the Cartesian space (see for example [9], [3], [21]). A task function isomorphic to the camera pose is built. As far as we know, except for some special "ad hoc" target [8], the isomorphism is generally believed true without any formal proof. The real existence of the isomorphism avoids situations where the task function is null and the camera is not well positioned [6]. In general, the task function is built using simple image features such as interest points coordinates. Since the control is done in the image, the target has much more chance to remain visible in the image.

- 2D 1/2 visual servoing: the task function $\mathbf{e}(\mathbf{q}, t)$ is expressed in the Cartesian space and in the image, i.e. the rotation error is estimated explicitly from a homography matrix and the translation error is expressed in the image (see for example [17], [13]). These visual servoing approaches make it possible not only to decouple the rotation and the translation control but also to perform the control in the image. It is possible with this approach to demonstrate the stability and the robustness of the control law [17].

The common drawback of all approaches is that in any case some information of the observed target is needed. In the 2D 1/2 visual servoing and 3D visual servoing, the pose reconstruction using the homography estimation is not unique (2 different solutions are possible). In order to choose the right solution, it is necessary to know an approximation of the normal vector to the target plane (or obtaining it from a cumbersome on-line estimation). In the 2D visual servoing, some 3D information (e.g. the depths when the features are points) is necessary to have a stable control law [19], [22].

In this paper, we present a new 2D visual servoing method that makes it possible to control the robot by building a task function isomorphic to the camera pose in the Cartesian space. In order to introduce our approach, we consider in this

paper planar targets with unknown 3D information (i.e. the normal vector to the target plane is unknown). In this case, the projective transformation linking two images of a plane is a homography. The method can be easily generalized to non-planar targets since it is always possible to compute a homography related to a virtual plane attached to the non-planar targets [18]. We have demonstrated that it exists an isomorphism between a task function $\mathbf{e}$ and the camera pose in the Cartesian space (i.e. the task function $\mathbf{e}$ is null, if and only if the camera is back to the reference pose). Contrarily to the standard 2D visual servoing, we have demonstrated that we do not need 3D information in order to guarantee the stability of the control law. The computation of the control law is quite simple (neither an interaction matrix estimation nor a homography decomposition is needed) and does not need any measure of the 3D structure of the observed target.

II. THEORETICAL BACKGROUND

As already mentioned in the introduction, we are interested in the positioning task of a camera mounted on a robot. The objective is to control the current camera frame $\mathcal{F}$ in order to reach a reference frame $\mathcal{F}^*$. To do that, we suppose to have an image $\mathcal{I}^*$ of the target, acquired in the reference pose, and a current image $\mathcal{I}$, acquired in the current pose, of same target acquired in real-time.

A. Projection model

Let $\mathcal{P}$ be a 3D point having Cartesian coordinates $\boldsymbol{\mathcal{X}} = [X, Y, Z]^\top$ in the current frame $\mathcal{F}$ (see Figure 1). The point can be projected on the unit sphere $\mathcal{S}$ in a 3D point having coordinates $\boldsymbol{\mathcal{X}}_s = [X_s, Y_s, Z_s]^\top$:

$$\boldsymbol{\mathcal{X}}_s = \frac{1}{\rho}\boldsymbol{\mathcal{X}} \tag{1}$$

where $\rho = \|\boldsymbol{\mathcal{X}}\|$. Following the central catadioptric camera projection models proposed in [1], [11] and [2], we can describe all omnidirectional images by projecting the point $\boldsymbol{\mathcal{X}}_s$ on the sphere from $\mathcal{C}_p$ to a point $\mathbf{m} = [x, y, 1]^\top$ on a virtual plane:

$$\mathbf{m} = \hbar(\boldsymbol{\mathcal{X}}_s) = \begin{bmatrix} \dfrac{X_s}{Z_s - \xi} & \dfrac{Y_s}{Z_s - \xi} & 1 \end{bmatrix}^\top \tag{2}$$

where ξ is a positive parameter ($0 \leq \xi \leq 1$) defining the geometry of the mirror (see TableI). Finally, the virtual point is projected on the image plane into the point $\mathbf{p} = [u, v, 1]^\top$:

$$\mathbf{p} = \mathbf{K}\mathbf{m} \tag{3}$$

where $\mathbf{K}$ is a triangular matrix containing the camera intrinsic parameters and another mirror parameter η (see TableI):

$$\mathbf{K} = \begin{bmatrix} f\,\eta & f\,\eta\,s & u_0 \\ 0 & f\,\eta\,r & v_0 \\ 0 & 0 & 1 \end{bmatrix} \tag{4}$$

u_0 and v_0 are the coordinates of the principal point (in pixels), f is the focal length measured in pixel, s is the skew and r is

the aspect ratio. As already mentioned, the parameters ξ and η define the geometry of the mirror (see table I).

	Equation	ξ	η
Parabolic	$\rho = Z + 2p$	1	$-2p$
Hyperbolic	$\dfrac{(Z+\frac{d}{2})^2}{a^2} - \dfrac{X^2}{b^2} - \dfrac{Y^2}{b^2} = 1$	$\dfrac{d}{\sqrt{d^2+4p^2}}$	$\dfrac{-2p}{\sqrt{d^2+4p^2}}$
Elliptic	$\dfrac{(Z+\frac{d}{2})^2}{a^2} + \dfrac{X^2}{b^2} + \dfrac{Y^2}{b^2} = 1$	$\dfrac{d}{\sqrt{d^2+4p^2}}$	$\dfrac{2p}{\sqrt{d^2+4p^2}}$

p and d are mirror parameters
$a = 1/2(\sqrt{d^2+4p^2} \pm 2p)$, '$-$' for the hyperbola, '$+$' for the ellipse
$b = \sqrt{p(\sqrt{d^2+4p^2} \pm 2p)}$, '$-$' for the hyperbola, '$+$' for the ellipse

TABLE I

MIRROR PARAMETERS.
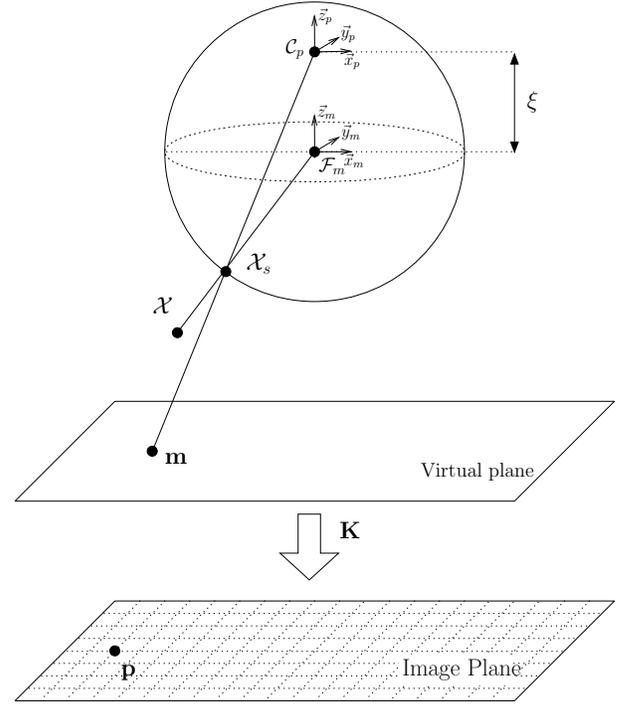
Fig. 1. Projection model for central catadioptric cameras

From a point $\mathbf{p}$ measured in the image, it is possible to compute its projection on the virtual plane $\mathbf{m} = \mathbf{K}^{-1}\mathbf{p}$ and then its projection on the unit sphere:

$$\boldsymbol{\mathcal{X}}_s = \hbar^{-1}(\mathbf{m}) = [\gamma x, \gamma y, \gamma + \xi]^\top$$

where $\gamma = -\dfrac{\xi + \sqrt{\xi^2 + (1-\xi^2)\|\mathbf{m}\|^2}}{\|\mathbf{m}\|^2} = -\dfrac{\xi + \sqrt{1 + (1-\xi^2)(x^2+y^2)}}{x^2+y^2+1}$.

B. Homography from two spherical projections

Let $\mathbf{R} \in \mathbb{SO}(3)$ and $\mathbf{t} \in \mathbb{R}^3$ be respectively the rotation and the translation between the current frame $\mathcal{F}$ and the reference frame $\mathcal{F}^*$ (see Figure2). The coordinates of the point $\mathcal{P}$ are $\boldsymbol{\mathcal{X}}^* = [X^*, Y^*, Z^*]^\top$ in the reference frame $\mathcal{F}^*$ while in the current frame $\mathcal{F}$ they are:

$$\boldsymbol{\mathcal{X}} = \mathbf{R}\boldsymbol{\mathcal{X}}^* + \mathbf{t} \tag{5}$$
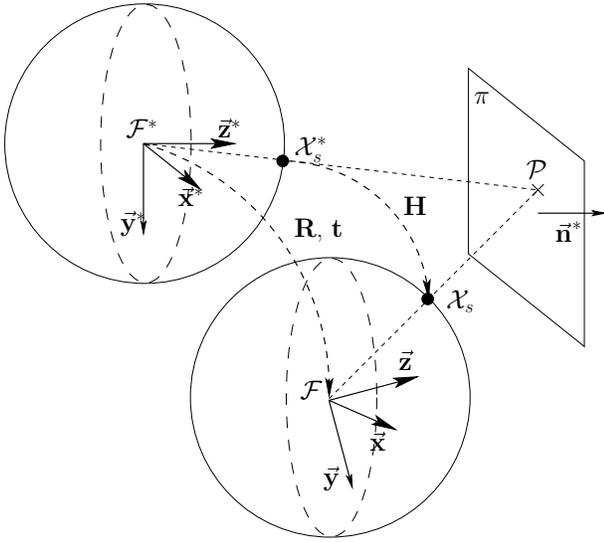
Fig. 2. Homography from two spherical projections.

Let $\mathbf{u} = [u_x, \; u_y, \; u_z]^\top$ be the unit vector corresponding to the rotation $\mathbf{R}$ and let θ ($\theta \in]-\pi, \pi[$) be the angle of the rotation $\mathbf{R}$. The rotation $\mathbf{R}$ can be written as the exponential matrix of an antisymmetric matrix:

$$\mathbf{R} = \exp(\theta \, [\mathbf{u}]_\times) \tag{6}$$

where exp is the matrix exponential function and $[\mathbf{u}]_\times$ is the antisymmetric matrix associated to the vector $\mathbf{u}$. The point $\mathcal{P}$ is projected on the reference unit sphere $\mathcal{S}^*$ into the point $\boldsymbol{\mathcal{X}}_s^* = [X_s^*, \; Y_s^*, \; Z_s^*]^\top$ where:

$$\boldsymbol{\mathcal{X}}_s^* = \frac{1}{\rho^*} \boldsymbol{\mathcal{X}}^* \tag{7}$$

and $\rho^* = \|\boldsymbol{\mathcal{X}}^*\|$. Let us suppose that $\mathcal{P}$ belongs to a plane π. Let d^* be the distance between π and the center of the sphere. Let $\mathbf{n}^*$ be a normal vector to π such that $\|\mathbf{n}^*\| = \frac{1}{d^*}$. Then, we have:

$$\mathbf{n}^{*\top} \boldsymbol{\mathcal{X}}^* = 1 \tag{8}$$

Using the equations (1), (5), (7) and (8), we can find the relationship between $\boldsymbol{\mathcal{X}}_s$ and $\boldsymbol{\mathcal{X}}_s^*$:

$$\frac{\rho}{\rho^*} \boldsymbol{\mathcal{X}}_s = \mathbf{H} \boldsymbol{\mathcal{X}}_s^* \tag{9}$$

where the homography matrix $\mathbf{H}$ is:

$$\mathbf{H} = \mathbf{R} + \mathbf{t}\mathbf{n}^{*\top} \tag{10}$$

Note that $\det(\mathbf{H}) > 0$, otherwise the camera has moved through the 3D plane and the target is not visible in the image any more. It is possible to compute $\mathbf{H}$ from two images $\mathcal{I}$ and $\mathcal{I}^*$ of a planar target. At least four pairs of corresponding points $\{\boldsymbol{\mathcal{X}}_{si}^*, \; \boldsymbol{\mathcal{X}}_{si}\}$, $i \in \{1, \; 2, \; 3, \; 4\}$ are necessary to compute $\mathbf{H}$ up to scale factor. The reconstruction of the camera displacement ($\mathbf{R}$ and $\mathbf{t}$ from $\mathbf{H}$) is not unique [10]. Generally, four triplets $\{\mathbf{R}_i, \; \mathbf{t}_i, \; \mathbf{n}_i^*\}$, $i \in \{1, \; 2, \; 3, \; 4\}$ are possible, two of which are physically admissible. An approximation of the normal vector $\mathbf{n}^*$ allows to choose the right solution.

III. VISUAL SERVOING WITH OMNI-CAMERAS

The objective of this paper is to design a new visual servoing method that does not need any measure of the structure of the observed target. Thus, we need to define an isomorphism between the information measure in the reference and current images and the camera pose. Then, we build a control law that depends on image information only.

A. A task function isomorphic to the camera pose

The two frames $\mathcal{F}$ et $\mathcal{F}^*$ coincide if and only if the matrix $\mathbf{H}$ is the identity matrix. We build, using $\mathbf{H}$, a task function $\mathbf{e} \in \mathbb{R}^6$ which is locally (since we have restricted $\theta \neq \pm\pi$) isomorphic to the camera pose. Thus, we have that $\mathbf{e}$ is zero if and only if the camera is in the reference pose.

Theorem 1: Task function isomorphism.
Let $\boldsymbol{\mathcal{X}}_s^*$ be the coordinates of a certain point on the sphere in the reference frame $\mathcal{F}^*$. The following task function:

$$\mathbf{e} = \left[\begin{array}{c} \mathbf{e}_\nu \\ \mathbf{e}_\omega \end{array} \right] \; with \; \left\{ \begin{array}{l} \mathbf{e}_\nu = (\mathbf{H} - \mathbf{I}) \boldsymbol{\mathcal{X}}_s^* \\ [\mathbf{e}_\omega]_\times = \mathbf{H} - \mathbf{H}^\top \end{array} \right. \tag{11}$$

is isomorphic to the camera pose, i.e. $\mathbf{e} = \mathbf{0}$, if and only if, $\theta = 0$ et $\mathbf{t} = \mathbf{0}$.

The proof of this theorem is given in the Appendix. The vector $\mathbf{e}$ can be computed completely from only the two images $\mathcal{I}$ et $\mathcal{I}^*$, i.e. without measuring the model of the target ($\mathbf{n}^*$ and ρ^*) and without decomposing the homography matrix. We can demonstrate that the task function vector can also be written as follows:

$$\mathbf{e} = \left[\begin{array}{c} \mathbf{e}_\nu \\ \mathbf{e}_\omega \end{array} \right] = \left[\begin{array}{c} (\mathbf{t} + (\mathbf{R} - \mathbf{I}) \boldsymbol{\mathcal{X}}^*)/\rho^* \\ 2\sin(\theta)\mathbf{u} + [\mathbf{n}^*]_\times \mathbf{t} \end{array} \right] \tag{12}$$

If we have $\mathbf{e}_\nu = \mathbf{0}$, then the two projections $\boldsymbol{\mathcal{X}}^*$ and $\boldsymbol{\mathcal{X}}$ of the same 3D point $\mathcal{P}$ coincide with each other. And if we have $\mathbf{e}_\omega = \mathbf{0}$, then the homography matrix $\mathbf{H}$ is symmetric.

B. The control law

The relationship between the derivative of the task function $\dot{\mathbf{e}}$ and the camera translation velocity $\boldsymbol{\nu}$ and the camera rotation velocity $\boldsymbol{\omega}$ is:

$$\dot{\mathbf{e}} = \mathbf{L} \left[\begin{array}{c} \boldsymbol{\nu} \\ \boldsymbol{\omega} \end{array} \right] \tag{13}$$

where the (6×6) interaction matrix $\mathbf{L}$ can be written as follows:

$$\mathbf{L} = \left[\begin{array}{cc} 1/\rho^* & -[\mathbf{e}_\nu + \boldsymbol{\mathcal{X}}_s^*]_\times \\ [\mathbf{n}^*]_\times & -[\mathbf{n}^*]_\times [\mathbf{t}]_\times + 2\mathbf{L}_\omega \end{array} \right] \tag{14}$$

and where the matrix $\mathbf{L}_\omega$ is:

$$\mathbf{L}_\omega = \mathbf{I} - \frac{\sin(\theta)}{2} [\mathbf{u}]_\times - \sin^2\left(\frac{\theta}{2}\right) (2\mathbf{I} + [\mathbf{u}]_\times^2) \tag{15}$$

The computation of the interaction matrix is given in the Appendix. In this paper, we propose a vision-based control law which is locally stable as stated by the following theorem:

Theorem 2: Local stability.
The following control law:

$$\left[\begin{array}{c} \boldsymbol{\nu} \\ \boldsymbol{\omega} \end{array} \right] = - \left[\begin{array}{c} \lambda_\nu \mathbf{e}_\nu \\ \lambda_\omega \mathbf{e}_\omega \end{array} \right] \tag{16}$$

with $\lambda_\nu > 0$ and $\lambda_\omega > 0$ is locally stable.

The proof of the theorem is given in the Appendix. The control law depends only on the task function $\mathbf{e}$ and can be completely computed from the two images $\mathcal{I}$ et $\mathcal{I}^*$. The interaction matrix $\mathbf{L}$ does not need to be estimated. It is only useful to prove analytically the control law stability. With such control law, the task function $\mathbf{e}$ converges exponentially to $\mathbf{0}$. The local stability of the control law is guaranteed for all $\mathbf{n}^*$ and for all $\boldsymbol{\mathcal{X}}_s$. By choosing $\lambda_\nu > 0$ and $\lambda_\omega > 0$ such that $\lambda_\nu \neq \lambda_\omega$, one can make $\mathbf{e}_\nu$ and $\mathbf{e}_\omega$ converge at different speeds.

IV. SIMULATION RESULTS

We have simulated a positioning task with an omni-directional camera mounted on a robot. In the first simulation, the mirror is parabolic while in the second simulation the mirror is hyperbolic. We consider 5 features points on a planar target. A reference image is stored and the robot is moved to its initial pose. We suppose to be able to match the current features with the reference ones and to be able to track them during the servoing. In both simulations, we apply the control law in equation (16) with $\lambda_\nu = \lambda_\omega = 1$. Indeed, since the homography matrix is computed from the points reprojected on the sphere, the same control law can be applied whatever mirror is used. It is important to notice again that we have not used any knowledge on the plane (e.g. its normal vector) to compute the control law in both simulations.

A. Parabolic mirror

In the first simulation, the displacement of the robot is $\mathbf{t} = [-0.5, 1.0, -1.0]^\top$ (in meters) and $\mathbf{r} = [\pi/12, \pi/12, -\pi/6]^\top$ (in radians). Figure 3 shows the results of the positioning task. The trajectories of the points in the image are illustrated in Figure 3(a). When the current points coincide with the reference ones, the robot is back to the reference pose. The control law is stable (see Figure 3(b)) and both translation and rotation errors converge to zero (see Figures 3(c) and Figures 3(d)).

B. Hyperbolic mirror

In the second simulation, the mirror is hyperbolic and the initial displacement is much bigger than the initial displacement in the previous simulation: $\mathbf{t} = [-1.0, 2.0, -2.0]^\top$ (in meters) and $\mathbf{r} = [\pi/5, -\pi/6, \pi/3]^\top$ (in radians). Despite Theorem 2 concerns only local stability (i.e. for small displacements), we can see in these simulations that the control law is stable even for large displacements (see Figure 4(b)) and the translation and rotation errors converge to zero again (see Figures 4(c) and Figures 4(d)). Finally, Figure 4(a) shows the trajectories of the points in the image.

(a) Trajectories in the image   (b) Control law

(c) Translation error   (d) Rotation error
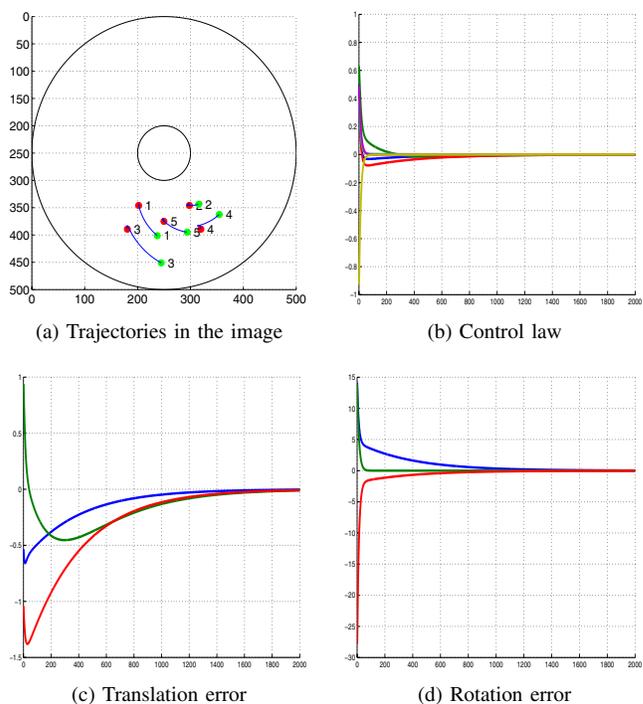
Fig. 3. Simulation: Positioning an omni-directional camera with a parabolic mirror with respect to an unknown planar target without using any approximation on it 3D parameters.

(a) Trajectories in the image   (b) Control law

(c) Translation error   (d) Rotation error
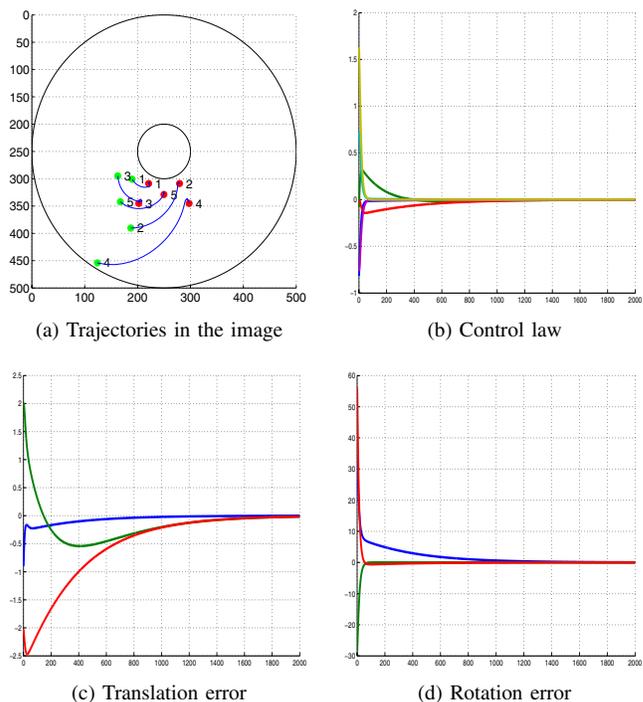
Fig. 4. Simulation: Positioning an omni-directional camera with a hyperbolic mirror with respect to an unknown planar target without using any approximation on it 3D parameters.

V. DISCUSSIONS ET CONCLUSIONS

In this paper, we have presented for the first time a new approach to visual servoing for omni-directional cameras that do

not need any measure of the 3D information on the observed scene. Indeed, we have proven that it is possible to compute, from image data only, a task function that is isomorphic to the camera pose. We have also proposed a simple control law and proven its local stability. The simulations have shown that the stability region is very large (but unknown for the moment). A deeper stability analysis will be necessary to theoretically define the exact stability region. Meanwhile, we plan to use trajectory planning for very large camera displacements.

VI. APPENDIX

A. The task function is isomorphic to the camera pose

In order to simplify the proof of Theorem (1), we proof three simpler propositions.

Proposition 1:
The matrix $\mathbf{H}\mathbf{H}^\top$ has one eigenvalue equal to 1. The eigenvector corresponding to the eigenvalue is $\mathbf{v} = [\mathbf{R}\mathbf{n}^*]_\times \mathbf{t}$.

Proof of proposition 1:
Using equation (10), we have:

$$\mathbf{H}\mathbf{H}^\top = (\mathbf{R} + \mathbf{t}\mathbf{n}^{*\top})(\mathbf{R}^\top + \mathbf{n}^*\mathbf{t}^\top)$$

Since we have $\mathbf{R} \in \mathbb{SO}(3)$ then $\mathbf{R}\mathbf{R}^\top = \mathbf{I}$. Thus, we have:

$$\mathbf{H}\mathbf{H}^\top = \mathbf{I} + \mathbf{t}(\mathbf{R}\mathbf{n}^*)^\top + (\mathbf{R}\mathbf{n}^* + \|\mathbf{n}^*\|^2\mathbf{t})\mathbf{t}^\top$$

The matrix $\mathbf{H}\mathbf{H}^\top$ is the sum of $\mathbf{I}$ and a rank 2 matrix. Thus, one eigenvalue of $\mathbf{H}\mathbf{H}^\top$ is equal to 1. Setting $\mathbf{v} = [\mathbf{R}\mathbf{n}^*]_\times \mathbf{t}$, we have:

$$(\mathbf{R}\mathbf{n}^*)^\top \mathbf{v} = 0 \quad \text{and} \quad \mathbf{t}^\top \mathbf{v} = 0$$

showing that $\mathbf{v}$ is an eigenvector of $\mathbf{H}\mathbf{H}^\top$:

$$\mathbf{H}\mathbf{H}^\top \mathbf{v} = \mathbf{v}$$

Proposition 2:
If $\mathbf{H} = \mathbf{H}^\top$ and $\sin(\theta) \neq 0$, then $\mathbf{n}^{*\top} \mathbf{u} = 0$, $\mathbf{t}^\top \mathbf{u} = 0$ and $\mathbf{n}^{*\top} \mathbf{v} = 0$ (where $\mathbf{v} = [\mathbf{R}\mathbf{n}^*]_\times \mathbf{t}$).

Proof of proposition 2:
If we have $\mathbf{H} = \mathbf{H}^\top$, then we have:

$$2\sin(\theta)\mathbf{u} + [\mathbf{n}^*]_\times \mathbf{t} = \mathbf{0} \qquad (17)$$

By multiplying each side of the equation (17) by $\mathbf{n}^{*\top}$, we obtain:

$$2\sin(\theta)\mathbf{n}^{*\top}\mathbf{u} = \mathbf{0}$$

Since we have supposed that $\sin(\theta) \neq 0$, we have:

$$\mathbf{n}^{*\top}\mathbf{u} = 0$$

Similarly, by multiplying each side of the equation (17) by $\mathbf{t}^\top$, we obtain:

$$\mathbf{t}^\top \mathbf{u} = 0$$

Finally, using the Rodriguez formula for the rotation matrix, we have:

$$\begin{aligned}
\mathbf{R}\mathbf{n}^* &= \left(\mathbf{I} + \sin(\theta)\left[\mathbf{u}\right]_\times + 2\cos^2\left(\frac{\theta}{2}\right)[\mathbf{u}]_\times^2\right)\mathbf{n}^* \\
&= \mathbf{n}^* + \sin(\theta)\left[\mathbf{u}\right]_\times \mathbf{n}^* + 2\cos^2\left(\frac{\theta}{2}\right)[\mathbf{u}]_\times^2 \mathbf{n}^* \\
&= \mathbf{n}^* + \sin(\theta)\left[\mathbf{u}\right]_\times \mathbf{n}^* + 2\cos^2\left(\frac{\theta}{2}\right)\left(\mathbf{u}\mathbf{u}^\top - \mathbf{I}\right)\mathbf{n}^*
\end{aligned}$$

If we have $\mathbf{n}^{*\top}\mathbf{u} = 0$, then we have:

$$\mathbf{R}\mathbf{n}^* = \mathbf{n}^* + \sin(\theta)\left[\mathbf{u}\right]_\times \mathbf{n}^* - 2\cos^2\left(\frac{\theta}{2}\right)\mathbf{n}^* \qquad (18)$$

The antisymmetric matrix associated to the vector $\mathbf{R}\mathbf{n}^*$ is:

$$[\mathbf{R}\mathbf{n}^*]_\times = [\mathbf{n}^*]_\times + \sin(\theta)\left[[\mathbf{u}]_\times \mathbf{n}^*\right]_\times - 2\cos^2\left(\frac{\theta}{2}\right)[\mathbf{n}^*]_\times$$

and since $\left[[\mathbf{u}]_\times \mathbf{n}^*\right]_\times = \mathbf{n}^*\mathbf{u}^\top - \mathbf{u}\mathbf{n}^{*\top}$, we can write:

$$[\mathbf{R}\mathbf{n}^*]_\times = [\mathbf{n}^*]_\times + \sin(\theta)\left(\mathbf{n}^*\mathbf{u}^\top - \mathbf{u}\mathbf{n}^{*\top}\right) - 2\cos^2\left(\frac{\theta}{2}\right)[\mathbf{n}^*]_\times$$

By multiplying both sides of the equation by $\mathbf{n}^{*\top}$, we obtain:

$$\mathbf{n}^{*\top}[\mathbf{R}\mathbf{n}^*]_\times = \|\mathbf{n}^*\|^2 \sin(\theta)\mathbf{u}^\top \qquad (19)$$

By multiplying both sides of the equation by $\mathbf{t}$, we obtain:

$$\mathbf{n}^{*\top}[\mathbf{R}\mathbf{n}^*]_\times \mathbf{t} = \|\mathbf{n}^*\|^2 \sin(\theta)\mathbf{u}^\top \mathbf{t}$$

Since $\mathbf{u}^\top \mathbf{t} = 0$, then we prove that:

$$\mathbf{n}^{*\top}\mathbf{v} = 0$$

Proposition 3:
If $\mathbf{H} = \mathbf{H}^\top$, $\mathbf{v} = [\mathbf{R}\mathbf{n}^*]_\times \mathbf{t} = \mathbf{0}$ and $\sin(\theta) \neq 0$ then $\det(\mathbf{H}) = -1$.

Proof of proposition 3:
If $\mathbf{v} = [\mathbf{R}\mathbf{n}^*]_\times \mathbf{t} = \mathbf{0}$ then it exists $\alpha \in \mathbb{R}^*$ such that:

$$\mathbf{t} = \alpha\mathbf{R}\mathbf{n}^*$$

From equation (19), we obtain:

$$[\mathbf{n}^*]_\times \mathbf{R}\mathbf{n}^* = \left(\mathbf{n}^{*\top}[\mathbf{R}\mathbf{n}^*]_\times\right)^\top = \|\mathbf{n}^*\|^2 \sin(\theta)\mathbf{u} \qquad (20)$$

Then, from equation (17) and equation (20), we obtain:

$$2\sin(\theta)\mathbf{u} = -[\mathbf{n}^*]_\times \mathbf{t} = -\alpha[\mathbf{n}^*]_\times \mathbf{R}\mathbf{n}^* = -\alpha\|\mathbf{n}^*\|^2 \sin(\theta)\mathbf{u}$$

By multiplying both sides of this equation by $\mathbf{u}^\top$, we obtain:

$$2\sin(\theta) = -\alpha\sin(\theta)\|\mathbf{n}^*\|^2$$

Since we supposed $\sin(\theta) \neq 0$, then we can write:

$$\alpha = -\frac{2}{\|\mathbf{n}^*\|^2}$$

and finally the determinant of the matrix $\mathbf{H}$ verifies:

$$\det(\mathbf{H}) = 1 + \mathbf{n}^{*\top}\mathbf{R}^\top \mathbf{t} = 1 + \alpha\|\mathbf{n}^*\|^2 = -1$$

Having a matrix $\mathbf{H}$ with negative determinant means that current frame $\mathcal{F}$ is on the opposite side of the target plane.

This is impossible since it means that we cannot see the target in the image any more. This is the reason why $\det(\mathbf{H}) > 0$.

Proof of theorem 1:

It is evident that if $\theta = 0$ and $\mathbf{t} = \mathbf{0}$ then $\mathbf{e} = \mathbf{0}$. We must prove now that if $\mathbf{e} = \mathbf{0}$, then $\theta = 0$ and $\mathbf{t} = \mathbf{0}$. Let us suppose that $\mathbf{e} = \mathbf{0}$. It is evident that if $\theta = 0$ then $\mathbf{t} = \mathbf{0}$ and if $\mathbf{t} = \mathbf{0}$ then $\theta = 0$. Now, let us suppose that $\mathbf{e} = \mathbf{0}$ and $\mathbf{t} \neq \mathbf{0}$ and $\theta \neq 0$. If $\mathbf{e}_\nu = \mathbf{0}$ then $\mathbf{H}\boldsymbol{\mathcal{X}}_s^* = \boldsymbol{\mathcal{X}}_s^*$. Thus, $\mathbf{H}$ has an eigenvalue equal to 1 and the vector $\boldsymbol{\mathcal{X}}_s^*$ is the corresponding eigenvector. The vector $\boldsymbol{\mathcal{X}}_s^*$ is also eigenvector corresponding to the eigenvalue 1 of the matrix $\mathbf{H}^2$. Since $\mathbf{e}_\omega = \mathbf{0}$ then $\mathbf{H} = \mathbf{H}^\top$ and $\mathbf{H}^2 = \mathbf{H}\mathbf{H}^\top$. Given Proposition 1, $\boldsymbol{\mathcal{X}}_s^*$ is then collinear to the vector $\mathbf{v} = [\mathbf{R}\mathbf{n}^*]_\times \mathbf{t}$. Since $\det(\mathbf{H}) > 0$, this vector is different from zeros (see Proposition 3). On the other hand, Proposition 2 shows that in this case $\mathbf{n}^{*\top}\boldsymbol{\mathcal{X}}_s^* = \rho^* = 0$. This is impossible since by definition $\rho^* > 0$. Thus, it is impossible that $\mathbf{e} = \mathbf{0}$ and $\mathbf{t} \neq \mathbf{0}$, $\theta \neq 0$.

B. The interaction matrix

Using equation (12), we have:

$$
\begin{aligned}
\dot{\mathbf{e}}_\nu &= (\dot{\mathbf{t}} + \dot{\mathbf{R}}\boldsymbol{\mathcal{X}}^*)/\rho^* \\
&= (\boldsymbol{\nu} + [\boldsymbol{\omega}]_\times \mathbf{t} + [\boldsymbol{\omega}]_\times \mathbf{R}\boldsymbol{\mathcal{X}}^*)/\rho^* \\
&= \boldsymbol{\nu}/\rho^* + [\boldsymbol{\omega}]_\times (\mathbf{t} + \mathbf{R}\boldsymbol{\mathcal{X}}^*)/\rho^* \\
&= \boldsymbol{\nu}/\rho^* + [\boldsymbol{\omega}]_\times (\mathbf{e}_\nu + \boldsymbol{\mathcal{X}}_s^*) \\
&= \boldsymbol{\nu}/\rho^* - [\mathbf{e}_\nu + \boldsymbol{\mathcal{X}}_s^*]_\times \boldsymbol{\omega}
\end{aligned}
$$

and:

$$
\begin{aligned}
\dot{\mathbf{e}}_\omega &= 2\frac{d\sin(\theta)\mathbf{u}}{dt} + [\mathbf{n}]_\times \dot{\mathbf{t}} \\
&= 2\mathbf{L}_\omega + [\mathbf{n}]_\times (\boldsymbol{\nu} + [\boldsymbol{\omega}]_\times \mathbf{t}) \\
&= [\mathbf{n}]_\times \boldsymbol{\nu} + (2\mathbf{L}_\omega - [\mathbf{n}]_\times [\mathbf{t}]_\times)\boldsymbol{\omega}
\end{aligned}
$$

Finally, we obtain equation (13) and the interaction matrix in equation (14).

C. Proof of the local stability of the control law

Proof of theorem 2:

After linearizing equation (13) about $\mathbf{e} = \mathbf{0}$, we obtain the following linear system:

$$
\dot{\mathbf{e}} = - \begin{bmatrix} \lambda_\nu/\rho^* & -\lambda_\omega [\boldsymbol{\mathcal{X}}_s^*]_\times \\ \lambda_\nu [\mathbf{n}^*]_\times & 2\lambda_\omega \mathbf{I} \end{bmatrix} \mathbf{e} = -\mathbf{L}_0 \mathbf{e}
$$

The eigenvectors of the constant matrix $\mathbf{L}_0$ are: 2λ, $4\rho^*$, $2\rho^* + \lambda + \sqrt{\lambda^2 + 4\rho^{*2}}$ (twice), $2\rho^* + \lambda - \sqrt{\lambda^2 + 4\rho^{*2}}$ (twice). where $\lambda = \lambda_\nu/\lambda_\omega$. Since $\lambda > 0$ and $\rho^* > 0$, the eigenvalues of matrix $\mathbf{L}_0$ are always positives. Consequently, the control law defined in equation (16) is always locally stable for any $\mathbf{n}^*$ and any $\boldsymbol{\mathcal{X}}_s^*$.

REFERENCES

[1] S. Baker and K. Nayar. A theory of single-viewpoint catadioptric image formation. *International Journal of Computer Vision*, 35(2):1–22, 1999.

[2] J. Barreto and H. Araujo. Geometric properties of central catadioptric line images. In *European Conf. on Computer Vision*, pages 237–251, 2002.

[3] J. P. Barreto, F. Martin, and R. Horaud. *Visual Servoing/Tracking Using Central Catadioptric Images*, chapter VI, pages 245–254. Springer Tracts in Advanced Robotics 5. Springer Verlag, experimental robotics viii edition, 2003.

[4] R. Basri, E. Rivlin, and I. Shimshoni. Visual homing: Surfing on the epipoles. In *IEEE Int. Conf. on Computer Vision*, pages 863–869, 1998.

[5] S. Benhimane and E. Malis. Vision-based control with respect to planar and non-planar objects using a zooming camera. In *IEEE International Conference on Advanced Robotics*, pages 991–996, 2003.

[6] F. Chaumette. Potential problems of stability and convergence in image-based and position-based visual servoing. In D. Kriegman, G. Hager, and A. Morse, editors, *The confluence of vision and control*, volume 237 of *LNCIS Series*, pages 66–78. Springer Verlag, 1998.

[7] G. Chesi, K. Hashimoto, D. Prattichizzo, and A. Vicino. A switching control law for keeping features in the field of view in eye-in-hand visual servoing. In *IEEE Int. Conf. on Robotics and Automation*, pages 3929–3934, 2003.

[8] N. J. Cowan and D. E. Chang. Toward geometric visual servoing. In A. Bicchi, H. Christensen, and D. Prattichizzo, editors, *Control Problems in Robotics*, volume 4 of *STAR, Springer Tracks in Advanced Robotics*, pages 233–248. Springer Verlag, 2002.

[9] B. Espiau, F. Chaumette, and P. Rives. A new approach to visual servoing in robotics. *IEEE Trans. on Robotics and Automation*, 8(3):313–326, 1992.

[10] O. Faugeras. *Three-dimensionnal computer vision: a geometric viewpoint*. MIT Press, Cambridge, MA, 1993.

[11] C. Geyer and K. Daniilidis. A unifying theory for central panoramic systems and practical applications. In *European Conf. on Computer Vision*, volume 2, pages 445–461, 2000.

[12] C. Geyer and K. Daniilidis. Mirrors in motion: Epipolar geometry and motion estimation. In *IEEE Int. Conf. on Computer Vision*, pages 766–773, 2003.

[13] H. Hadj Abdelkader, Y. Mezouar, N. Andreff, and P. Martinet. 2 1/2 d visual servoinf with central catadioptric cameras. In *IEEE Int. Conf. on Intelligent Robots and Systems*, 2005.

[14] K. Hashimoto. *Visual Servoing: Real Time Control of Robot manipulators based on visual sensory feedback*, volume 7 of *World Scientific Series in Robotics and Automated Systems*. World Scientific Press, Singapore, 1993.

[15] S. Hutchinson, G. D. Hager, and P. I. Corke. A tutorial on visual servo control. *IEEE Trans. on Robotics and Automation*, 12(5):651–670, 1996.

[16] H. C. Longuet-Higgins. A computer algorithm for reconstructing a scene from two projections. *Nature*, 293:133–135, 1981.

[17] E. Malis and F. Chaumette. Theoretical improvements in the stability analysis of a new class of model-free visual servoing methods. *IEEE Trans. on Robotics and Automation*, 18(2):176–186, 2002.

[18] E. Malis, F. Chaumette, and S. Boudet. 2 1/2 d visual servoing with respect to unknown objects through a new estimation scheme of camera displacement. *Int. Journal of Computer Vision*, 37(1):79–97, 2000.

[19] E. Malis and P. Rives. Robustness of image-based visual servoing with respect to depth distribution errors. In *IEEE International Conference on Robotics and Automation*, 2003.

[20] Y. Mezouar and F. Chaumette. Path planning for robust image-based control. *IEEE Trans. on Robotics and Automation*, 18(4):534–549, 2002.

[21] Y. Mezouar, H. Haj Abdelkader, P. Martinet, and F. Chaumette. Central catadioptric visual servoing from 3d straight lines. In *IEEE Int. Conf. on Intelligent Robots and Systems*, volume 1, pages 343–349, 2004.

[22] Y. Mezouar and E. Malis. Robustness of central catadioptric image-based visual servoing to uncertainties on 3d parameters. In *IEEE/RSJ International Conference on Intelligent Robots Systems*, 2004.

[23] C. Samson, M. Le Borgne, and B. Espiau. *Robot Control: the Task Function Approach*, volume 22 of *Oxford Engineering Science Series*. Clarendon Press, Oxford, UK, 1991.

[24] T. Svoboda and P. T. Epipolar geometry for central catadioptric cameras. *International Journal of Computer Vision*, 49(1):23–37, August 2002.

[25] C. Taylor, J. Ostrowski, and S. Jung. Robust vision-based pose control. In *IEEE Int. Conf. on Robotics and Automation*, pages 2734–2740, 2000.